INTERNATIONAL JOURNAL FOR NUMERICAL METHODS IN FLUIDS
Int. J. Numer. Meth. Fluids 2005; **47**:911–923
Published online 18 January 2005 in Wiley InterScience (www.interscience.wiley.com). DOI: 10.1002/fld.907

Dynamic structure subgrid-scale models for large eddy simulation

Sergei G. Chumakov*,† and Christopher J. Rutland

Department of Mechanical Engineering, University of Wisconsin-Madison, U.S.A.

SUMMARY

Large eddy simulation (LES) is based on separation of variable of interest into two parts—resolved and subgrid. The resolved part is obtained numerically using modified transport equation while the effect of the subgrid part is modelled using subgrid-scale (SGS) models. In this paper we present and discuss new one-equation LES models for SGS scalar flux, SGS scalar dissipation and SGS energy dissipation. The proposed models belong to a new family of SGS models—dynamic structure (DS) models. The DS models borrow the structure of the modelled term from the corresponding Leonard term, and a special scaling factor is then used which does not contain user-specified constants. The models are evaluated *a priori* using available DNS data for a non-reacting mixing layer and decaying isotropic turbulence; the evaluation results compare well with viscosity and similarity models. During the *a priori* tests, the DS models were found to perform better than dynamic viscosity and similarity models for various test-to-base filter size ratios and non-symmetric filters. For *a posteriori* evaluation, the models are implemented into a high-order finite-difference code and an LES of decaying isotropic turbulence is performed. The results match the data available from the literature and DNS simulations.

KEY WORDS: large eddy simulation; subgrid-scale modelling; scalar flux; scalar dissipation; energy dissipation; turbulence modelling

1. INTRODUCTION

Over the last several decades, large eddy simulation (LES) approach has been successfully applied to a variety of problems ranging from the weather prediction [1] to simulation of internal combustion engines [2]. The main advantage of LES is that it captures the unsteady effects of the modelled flow better than the Reynolds-Averaged Navier–Stokes (RANS)

*Correspondence to: Sergei G. Chumakov, Engineering Research Center, University of Wisconsin, 1011 Engineering Research Building, 1500 Engineering Dr., WI 53706 Madison, U.S.A.
†E-mail: sergei@erc.wisc.edu

Contract/grant sponsor: U.S. Army Research Office; contract/grant number: DAAD19-00-1-0487
Contract/grant sponsor: Air Force Office of Scientific Research; contract/grant number: F49620-02-1-0348

Received 27 April 2004
Revised 15 December 2004
Accepted 15 December 2004

approach, and yet does not require such extensive computational power as direct numerical simulation (DNS).

The essence of the LES approach is the separation of variables of interest like velocity, temperature, mixture fraction and other scalars, into resolved and unresolved parts. The resolved, or large-scale quantities are computed numerically using modified conservation equations. The unresolved, or subgrid, quantities are not directly available and thus their effect on the resolved scales must be modelled. The quality of subgrid models is most crucial for any LES computation.

The separation of scales is done by applying a spatial filter to the variable of interest. For any flow variable ϕ, it is postulated that $\phi = \bar{\phi} + \phi'$, where the resolved part $\bar{\phi}$ and unresolved part ϕ' are defined as $\bar{\phi} = \phi * G$ and $\phi' = \phi - \bar{\phi}$. Here, G is the filter function and must satisfy $\|G\|_1 = 1$, and '$*$' is the convolution operator. Also, some models require an additional filtering operation, which is referred to as 'test filtering'. Usually the test-filtered quantity is denoted by $\hat{\phi}$ and is defined as $\hat{\phi} = \phi * \hat{G}$, where $\hat{G}$ is called the test filter function.

The unresolved quantities are difficult to measure in experimental setup thus making *a priori* LES model evaluation difficult. An alternative consists of utilizing existing DNS results where all scales are resolved and thus the subgrid-scale (SGS) quantities are available by applying a straightforward filtering operation; this technique is used in this work.

We consider three new SGS models: for SGS scalar flux, SGS scalar dissipation, and SGS energy dissipation. Each of these three models is evaluated *a priori* using available DNS data for decaying isotropic turbulence and a non-reacting incompressible mixing layer. After that, to evaluate the momentum-related models *a posteriori*, LES simulations of isotropic decay is performed.

2. GOVERNING EQUATIONS AND MODELLED TERMS

The governing equations for LES are obtained by formally applying the spatial filtering procedure to the fundamental conservation equations [3]. The LES governing equations of interest are conservation of momentum and scalar

$$\frac{\partial \bar{u}_i}{\partial t} + \bar{u}_j \frac{\partial \bar{u}_i}{\partial x_j} = -\frac{\partial \bar{p}}{\partial x_i} + \nu \frac{\partial^2 \bar{u}_i}{\partial x_j \partial x_j} - \frac{\partial \tau_{ij}}{\partial x_j} \tag{1}$$

$$\frac{\partial \bar{\phi}}{\partial t} + \bar{u}_i \frac{\partial \bar{\phi}}{\partial x_i} = D \frac{\partial^2 \bar{\phi}}{\partial x_i \partial x_i} + \bar{\omega} - \frac{\partial \tau_{i\phi}}{\partial x_i} \tag{2}$$

Here, $\tau_{ij} = \overline{u_i u_j} - \bar{u}_i \bar{u}_j$ is the SGS momentum flux, ϕ is a generic scalar, $\tau_{i\phi} = \overline{u_i \phi} - \bar{u}_i \bar{\phi}$ is the SGS scalar flux, D is the diffusion coefficient, and $\bar{\omega}$ is the filtered source term for the scalar ϕ, e.g., due to chemistry. Both Equations (1) and (2) have unclosed terms which need to be modelled. Many models for τ_{ij} have been proposed and evaluated (for review, see Reference [4]). Fewer models have been proposed for $\tau_{i\phi}$.

Several models for τ_{ij} employ an auxiliary LES quantity—SGS kinetic energy [5–7] $k = (\overline{u_i u_i} - \bar{u}_i \bar{u}_i)/2$, for which an additional transport equation is solved

$$\frac{\partial k}{\partial t} + \bar{u}_i \frac{\partial k}{\partial x_i} = \nu \frac{\partial^2 k}{\partial x_i \partial x_i} - \varepsilon - \tau_{ij} \bar{S}_{ij} \tag{3}$$

Here, ε is the SGS energy dissipation, and $\bar{S}_{ij}$ is the resolved rate of strain tensor

$$\varepsilon = \nu \left[\overline{\frac{\partial u_i}{\partial x_j} \frac{\partial u_i}{\partial x_j}} - \frac{\partial \bar{u}_i}{\partial x_j} \frac{\partial \bar{u}_i}{\partial x_j} \right], \qquad \bar{S}_{ij} = \frac{1}{2} \left[\frac{\partial \bar{u}_i}{\partial x_j} + \frac{\partial \bar{u}_j}{\partial x_i} \right]$$

The SGS energy dissipation term is unclosed and thus needs to be modelled too.

In the models that we are going to present, we make use of another auxiliary quantity—the SGS scalar variance $\theta = \overline{\phi^2} - \bar{\phi}^2$, which is obtained from a separate transport equation. For the incompressible case, one of the forms of the transport equation for θ is given by [8]

$$\frac{\partial \theta}{\partial t} + \bar{u}_i \frac{\partial \theta}{\partial x_i} = 2D \frac{\partial^2 \theta}{\partial x_i \partial x_i} - \chi - 2\tau_{i\phi} \frac{\partial \bar{\phi}}{\partial x_i} + O(\Delta^4) \tag{4}$$

Here, D is the diffusion coefficient, Δ is the LES grid spacing, and χ denotes the SGS scalar dissipation

$$\chi = 2D \left[\overline{\frac{\partial \phi}{\partial x_i} \frac{\partial \phi}{\partial x_i}} - \frac{\partial \bar{\phi}}{\partial x_i} \frac{\partial \bar{\phi}}{\partial x_i} \right]$$

Thus, there are four terms to model: τ_{ij}, $\tau_{i\phi}$, ε, and χ. This work deals with models for the latter three terms. For the SGS momentum flux τ_{ij}, we use the following DS model [7, 9]:

$$\tau_{ij} \approx \frac{2k}{L_{mm}} L_{ij}, \quad L_{ij} = \widehat{\bar{u}_i \bar{u}_j} - \hat{\bar{u}}_i \hat{\bar{u}}_j \tag{5}$$

Here k is the SGS kinetic energy, and L_{ij} is the Leonard term.

3. FORMULATION OF THE MODELS

For the SGS scalar flux $\tau_{i\phi}$ we propose to use the following model:

$$\tau_{i\phi} \approx \frac{\theta}{\Theta} L_{i\phi} = \frac{\overline{\phi\phi} - \bar{\phi}\,\bar{\phi}}{\widehat{\bar{\phi}\,\bar{\phi}} - \hat{\bar{\phi}}\,\hat{\bar{\phi}}} \left[\widehat{\bar{u}_i \bar{\phi}} - \hat{\bar{u}}_i \hat{\bar{\phi}} \right] \tag{6}$$

Here, $\widehat{(\cdot)}$ denotes the test filtering, θ is the SGS scalar variance, $\Theta = \widehat{\bar{\phi}\,\bar{\phi}} - \hat{\bar{\phi}}\,\hat{\bar{\phi}}$ is the test-level SGS scalar variance, and $L_{i\phi} = \widehat{\bar{u}_i \bar{\phi}} - \hat{\bar{u}}_i \hat{\bar{\phi}}$ is the Leonard-type term for the SGS scalar flux. Note that the model can be derived in two ways. First, we can treat this model as a self-similarity model [10] with a particular form of scaling coefficient. Alternatively, we can start with the assumption $\tau_{i\phi} \approx c_i \theta$ and formally apply the Dynamic Procedure [11] in order to determine coefficients c_i. We then arrive to $c_i = L_{i\phi}/\Theta$.

For the SGS scalar dissipation χ, the following model is proposed:

$$\chi \approx C_\chi \frac{\theta}{\Theta} L_\chi \tag{7}$$

Here, L_χ is the Leonard-type term for the SGS scalar dissipation

$$L_\chi = 2D\left[\widehat{\frac{\partial\bar{\phi}}{\partial x_i}}\,\widehat{\frac{\partial\bar{\phi}}{\partial x_i}} - \widehat{\frac{\partial\bar{\phi}}{\partial x_i}}\,\widehat{\frac{\partial\bar{\phi}}{\partial x_i}}\right]$$

The form of the model was suggested by the self-similarity idea and the particular scaling factor of model (6) for $\tau_{i\phi}$. The recommended value for the constant C_χ, based on the *a priori* tests described later, is $C_\chi = 2$. Again, like with model (6), we can derive model (7) using Dynamic Procedure starting with $\chi \approx C_\chi f\theta$ and arriving to $f = L_\chi/\Theta$.

Finally, the proposed model for the SGS energy dissipation ε is

$$\varepsilon \approx \nu \cdot F \cdot L_\varepsilon = \nu \cdot F \cdot \left[\widehat{\frac{\partial\bar{u}_i}{\partial x_j}}\,\widehat{\frac{\partial\bar{u}_i}{\partial x_j}} - \widehat{\frac{\partial\bar{u}_i}{\partial x_j}}\,\widehat{\frac{\partial\bar{u}_i}{\partial x_j}}\right] \tag{8}$$

We shall try to determine the form of the scaling factor F from *a priori* tests described in the next section. It is currently a work in progress, and for the *a posteriori* test, a simple form of F, described later, is used.

We would like to consider the three models presented as ones that belong to a new class of SGS models—Dynamic Structure (DS) models. The DS models take the general structure of the modelled term from the corresponding Leonard-type term and then a particular form of the scaling factor is sought.

4. *A PRIORI* TESTS

4.1. *DNS data*

For *a priori* tests we used several sets of DNS data. The first set of DNS data was taken from the literature [12] and consisted of one snapshot of the velocity field in the triple-periodic $(2\pi)^3$ box with Reynolds number Re_λ based on Taylor microscale λ equal to 104. In our study this DNS data was used to evaluate the model for ε. The second set of data was generated by a finite-difference code to simulate the incompressible non-reacting mixing layer with temperature as a passive scalar [13]. This set of data was used to evaluate all presented models.

4.2. *SGS energy dissipation*

First, we conducted *a priori* test for the model (8) using the first set of DNS data. The proposed form of the scaling factor F is the following:

$$F = C_\varepsilon\left[\frac{2k}{L_{ii}}\right]^\gamma$$

Here, k is the SGS kinetic energy, L_{ij} is the Leonard term, and C_ε and γ are the constants to be determined from this *a priori* study.

Figure 1(a) presents the probability density functions (PDFs) for C_ε obtained for the case $\gamma = \frac{1}{2}$. Different curves refer to different combinations of the test and base filters. The numbers in parentheses refer to the size of the base and test filters in terms of the DNS grid spacing.

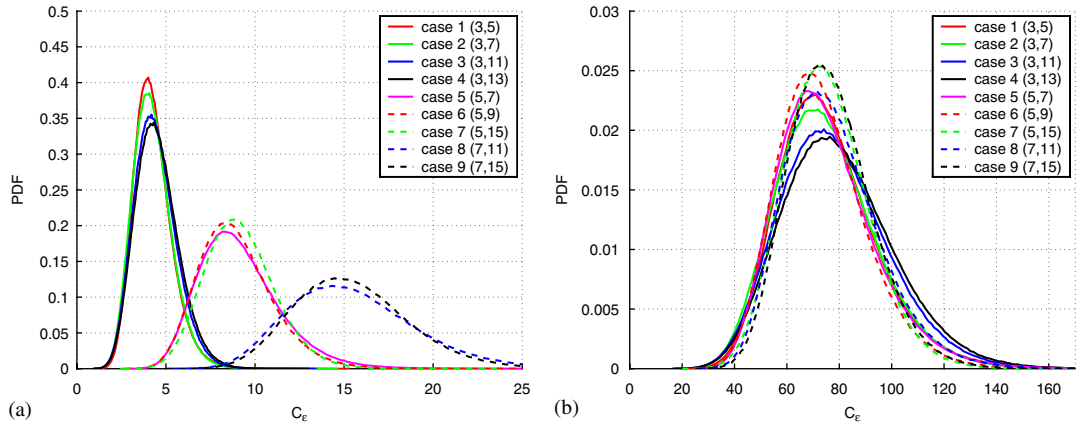

Figure 1. (a) PDFs for C_ε; and (b) $C_\varepsilon/\Delta^{3/2}$ for the case $\gamma = \frac{1}{2}$.

Figure 1(a) shows a clear dependence of C_ε on the base filter size Δ for $\gamma = \frac{1}{2}$. This motivated us to compute PDFs for $C_\varepsilon/\Delta^\zeta$ for various values of ζ. The resulting PDFs for the value of ζ equal to $\frac{3}{2}$ are presented in the Figure 1(b). The DNS data for isotropic turbulence [12] is used.

Evaluation of the model for ε using the data from DNS of a mixing layer shows similar trends, although the PDFs are not as perfectly aligned. The difference is attributed to a high degree of flow anisotropy present in the mixing layer.

Thus, the final form of the DS model for the SGS energy dissipation ε is as follows:

$$\varepsilon \approx \nu C \left[\frac{\Delta}{l}\right]^{3/2} \sqrt{\frac{2k}{L_{mm}}} \left[\widehat{\frac{\partial \bar{u}_i}{\partial x_j}} \widehat{\frac{\partial \bar{u}_i}{\partial x_j}} - \widehat{\frac{\partial \bar{u}_i}{\partial x_j}}\,\widehat{\frac{\partial \bar{u}_i}{\partial x_j}}\right] \tag{9}$$

where C is a scaling constant, l is a length scale, both to be determined in the future work.

4.3. *Scalar-related models*

In order to evaluate the scalar-related SGS models *a priori*, we used the second set of data from the DNS of an incompressible non-reacting mixing layer [13].

The DNS was conducted with the following parameters: the grid size of $481 \times 241 \times 16$ in the streamwise, transverse and spanwise directions, domain size of $120 \times 60 \times 9.6$, velocity ratio of $\frac{1}{3}$ and Reynolds number of 200. All lengths are normalized by the inlet vorticity thickness, and the temperature is used as a passive scalar. The simulation was conducted using a finite-difference non-dissipative code that is 11th order accurate in space and fifth-order accurate in time. A thorough accuracy study has been performed [13].

Similar to the case of the model for SGS energy dissipation, we compared performance of DS models (6) and (7) with two models found in the literature by varying the base and test filter sizes and dimensions. This, in our opinion, should test the models' robustness, i.e., whether the performance is affected by size and shape of base and test filters.

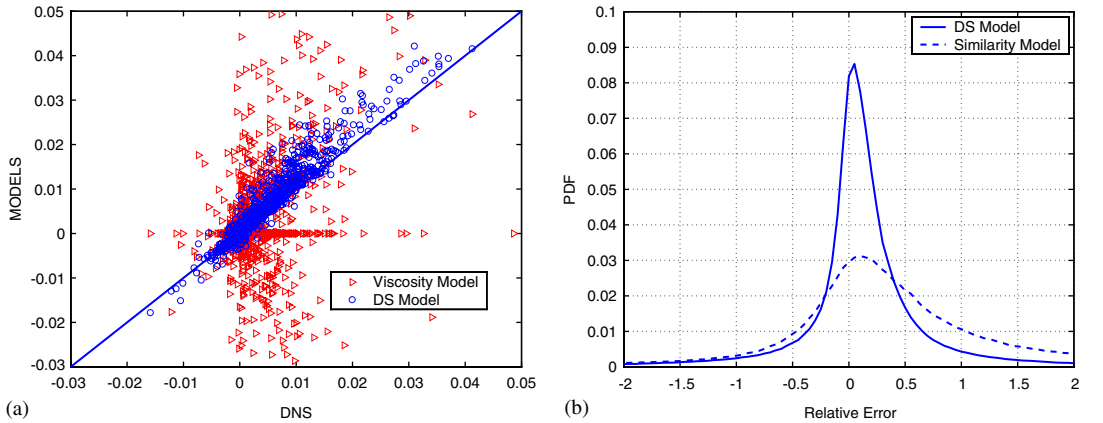

Figure 2. (a) Scatter plot of $\tau_{i\phi}$ computed from DNS data vs the DS model (circles) and dynamic viscosity model (triangles); and (b) PDFs of relative error for DS model (solid) and self-similarity model (dashed) for the SGS scalar flux $\tau_{i\phi}$.

Figure 2(a) presents the result of comparison of the DS model (6) for the SGS scalar flux with the common dynamic viscosity model given by [14, 15]

$$\tau_{i\phi} \approx -C\Delta^2 |\bar{S}_{ij}| \frac{\partial \bar{\phi}}{\partial x_i}$$

The figure shows the scatter plot of the modelled quantity calculated from the DNS data versus the value of the model. The advantage of the DS model is evident from the scatter plot—the points that correspond to the DS model lie much closer to the identity graph (the line) and the dispersion is much narrower.

A comparison was made of the DS model to a more successful model—scale-similarity model, which is given by [10]

$$\tau_{i\phi} \approx cL_{i\phi} \tag{10}$$

The value of the constant c was set to 1. This time a different sort of comparison was made. We calculated the PDF of relative error E for both models, defined as

$$E = \frac{\text{model} - \tau_{i\phi}}{\tau_{i\phi}}$$

The result is shown in Figure 2(b). The combination of the base and test filter sizes was chosen in such a way that it resulted in the best performance of the scale-similarity model (10).

The DS model shows a sharper and more narrow peak in the PDF of relative error and thus can be considered superior. Moreover, the DS model appeared to be more robust, i.e., it showed weaker dependence on the base and test-level filter sizes and shapes.

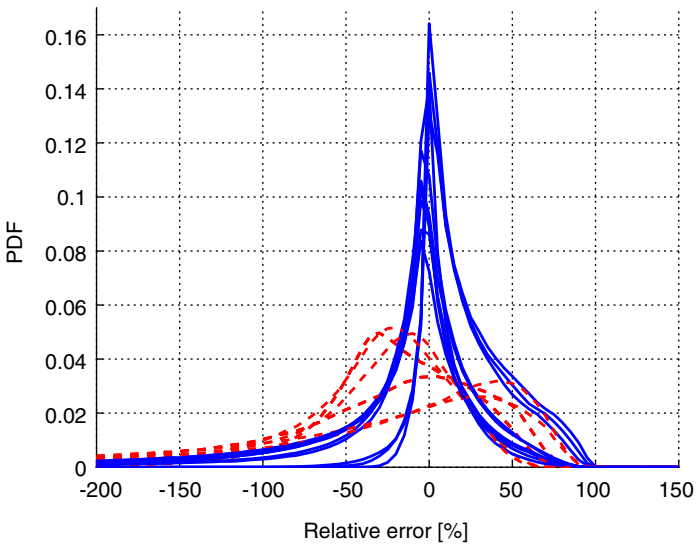

Figure 3. PDFs of relative error for DS model (solid) and momentum-based model (dashed) for the SGS scalar dissipation χ_0. Different lines correspond to different base and test filter combinations.

The same type of *a priori* test was conducted for the DS model for the SGS scalar dissipation. For comparison, a model based on the momentum analogy was chosen [16]

$$\chi_0 \equiv 2D\overline{\frac{\partial\phi}{\partial x_i}\frac{\partial\phi}{\partial x_i}} \approx 1.1\frac{\varepsilon}{k}\theta \tag{11}$$

This model, although criticized in the literature [17], was chosen for comparison due to its simplicity, relatively good performance and independence on spectral formulation, which broadens its applicability range.

For the comparison purposes, values of χ_0 were computed using both DS model (7) $\chi_0 \approx 2D\left[2\theta L_\chi/\Theta + \partial\bar{\phi}/\partial x_i \partial\bar{\phi}/\partial x_i\right]$ and momentum-based model (11) and then compared to the values of χ_0 obtained from the fully resolved DNS field.

We conducted the *a priori* comparison for several cases. The base and test filter sizes were varied, as were the filter shapes. This was done in order to test the robustness of both models. PDFs shown in Figure 3 were computed for various filter dimensions ranging from $3\Delta_g$ to $15\Delta_g$, and for filter shapes ranging from isotropic to highly asymmetric, e.g., $6\Delta_g \times 14\Delta_g \times 10\Delta_g$, where Δ_g is the DNS grid spacing. The performance of the momentum-based model appears to be strongly dependent on the chosen filter configuration, while the DS model seems to be almost unaffected by it. In our opinion, this shows that the DS model is more robust.

5. LES OF DECAYING ISOTROPIC TURBULENCE

5.1. Experimental and theoretical results

In an earlier work [8], we performed *a posteriori* testing of DS models by conducting LES of an incompressible mixing layer and matching the statistics from the LES run with ones obtained from DNS [13]. In this work, we evaluate the DS models by performing LES of decaying isotropic turbulence.

By decaying isotropic turbulence (DIT) we mean the flow that has zero mean velocity, is homogeneous and isotropic. Numerical simulation of DIT, although somewhat impractical for engineering applications, became a *de facto* standard test case for *a posteriori* evaluation of LES models. This might be attributed to the fact that of all turbulent flows, DIT is one of the most well studied. A lot of theoretical results are available [3, 18], and some widely recognized measurements and DNS simulation results are available in the literature [19–21].

Generally, two types of comparison to the experimental data can be made for *a posteriori* evaluation:

- Energy spectrum for different times, or more specifically, for different Re_λ;
- Rate of decay of kinetic energy in time.

The former is more suitable for DNS rather than LES since the LES and DNS energy spectra are quite different for non-cutoff filters (see Figure 4(a)). Thus the main comparison we are going to make is matching the energy decay rate in time. This is indeed a good test for both models for the SGS stress τ_{ij} and the SGS energy dissipation ε. This particular test evaluates the ability of both models to manage the energy budget between the resolved and unresolved scales, and unresolved and viscous scales as well. Energy transfer rates on both levels are closely related and both models must perform adequately to reproduce the experimental results.

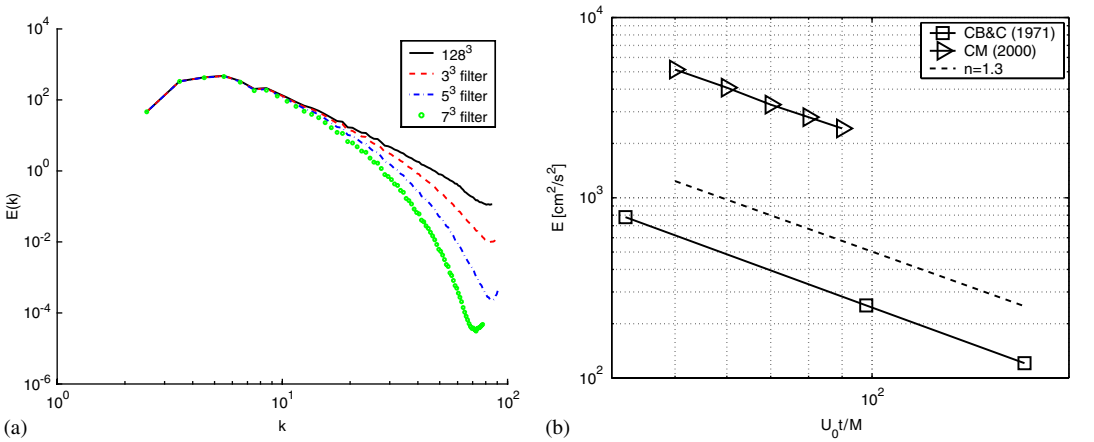

Figure 4. (a) Energy spectra for resolved [12] and filtered flow fields using non-cutoff filters of various sizes; and (b) Kinetic energy decay: experiments by Comte-Bellot and Corrsin [20] (squares) and Cerutti and Meneveau [21] (triangles). The exponent $n = 1.3$ is plotted for comparison.

In the current literature, when the LES of DIT is performed, usually the energy decay rate is compared to the experimental measurements of Comte-Bellot and Corrsin [20] on a non-logarithmic plot [5]. The type of comparison we are going to make differs from the one usually performed.

In an earlier paper, Comte-Bellot and Corrsin's [19] measurements suggested that the total energy decays as a power law, which, in the laboratory frame, can be written as

$$\frac{K}{U_0^2} = A\left[\frac{x - x_0}{M}\right]^{-n} \tag{12}$$

where K is the total kinetic energy, U_0 is the freestream velocity, A and M are constants, x is the streamwise co-ordinate, and x_0 is the virtual origin.

In general, the DIT exhibits two different types of behaviour: inertia-dominated in earlier stage, and viscosity-dominated in the final stage when Re_λ is low enough [3]. For the inertia-dominated period, only experimental measurements are known. The total kinetic energy clearly exhibits the power-law decay similar to (12). Both Comte-Bellot and Corrsin's data [20] and Cerutti and Meneveau's [21] data suggest $n = 1.29$. The values of the decay exponent n between 1.15 and 1.45 are reported in the literature but it has been suggested [22] that nearly all of the data are consistent with $n = 1.3$. Figure 4(b) shows the energy decay rate extracted from the experimental measurements by Comte-Bellot and Corrsin [20], and Cerutti and Meneveau [21]. The exponential decay rate for $n = 1.3$ is plotted for comparison.

The energy decay rate for the viscosity-dominated (final) period can be obtained analytically from the Karman–Howarth equation [18], which yields $E \propto t^{-5/2}$, which is in excellent agreement with existing experimental data. It is emphasized that this solution applies only to very low Reynolds numbers—much lower than is generally of interest. Thus, instead of trying to match the experimental data for the energy decay rate and power spectra, we are going to match the energy decay rate given by LES against the power law (12) with $n = 1.3$ for the inertia-dominated period, and $n = 2.5$ for the final period.

5.2. *LES results*

The following two sets of models have been tested *a posteriori*:

1. DS models

$$\tau_{ij} \approx \frac{2k}{L_{mm}} L_{ij}, \quad \varepsilon \approx \nu C_\varepsilon \frac{2k}{L_{mm}} \left[\widehat{\frac{\partial \bar{u}_i}{\partial x_j}}\,\widehat{\frac{\partial \bar{u}_i}{\partial x_j}} - \widehat{\frac{\partial \bar{u}_i}{\partial x_j}}\,\widehat{\frac{\partial \bar{u}_i}{\partial x_j}}\right]$$

2. The dynamic viscosity one-equation models (referred to as 'Localization models', or LM) [5, 6, 23]

$$\tau_{ij} \approx -0.05\,\Delta\sqrt{k}\,\bar{S}_{ij}, \quad \varepsilon \approx 1.0\,\frac{k^{3/2}}{\Delta}$$

Figures 5–7 present the results from LES runs. The first run, referred to as 'DS' in figures, uses the first set of models with an empirical constant $C_\varepsilon = 8$. The second run uses the second set of models and is referred to as 'LM' in the figures. For the LM set of models, the Dynamic Procedure can be applied in order to estimate the *a priori* given coefficients [5]. However,

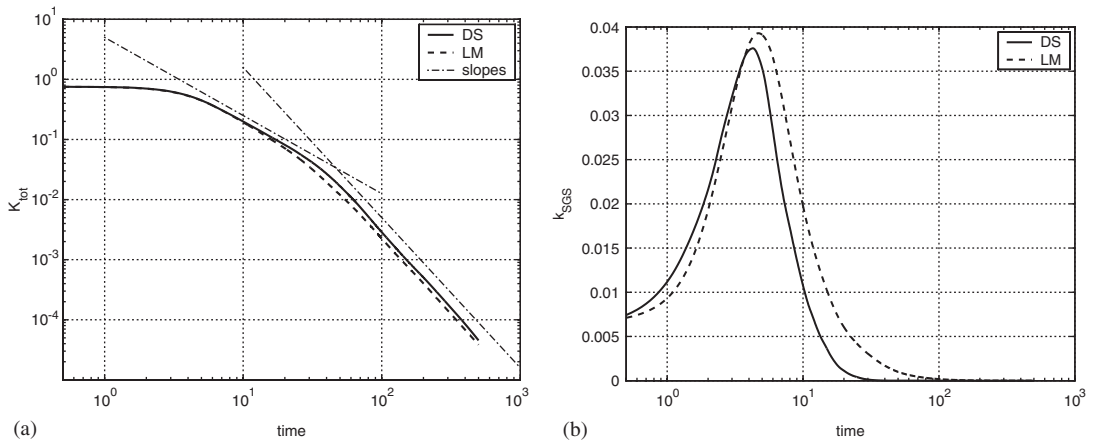

Figure 5. (a) Decay of total kinetic energy in time for DS and LM sets of models. Slopes for $n = 1.3$ and 2.5 are plotted; and (b) decay of the SGS kinetic energy in time for DS and LM sets of models.

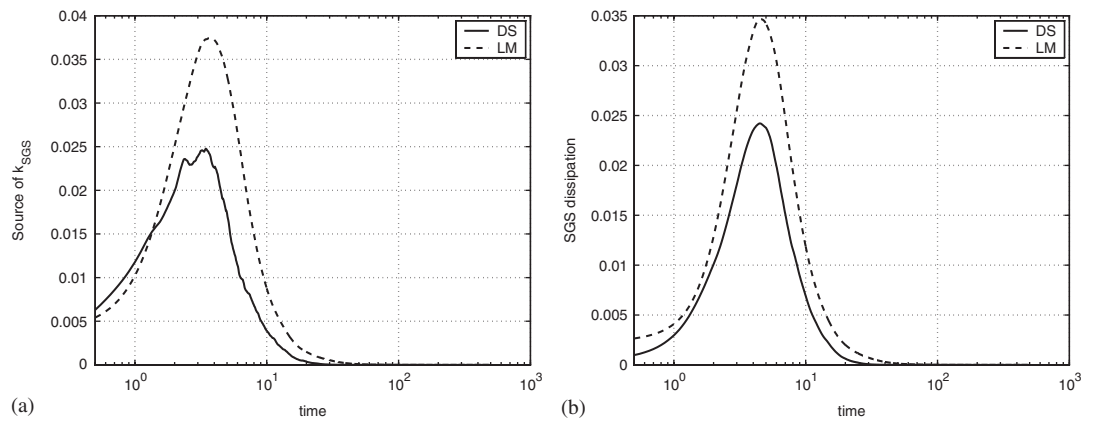

Figure 6. (a) Evolution of the energy transfer term in time for DS and LM sets of models; and (b) dissipation of SGS kinetic energy in time for DS and LM sets of models.

the resulting integral equation is not always solvable [7] thus we used constant coefficients that resulted in the best performance of the given set of models [23]. Both runs were performed using 32^3 computational grid.

Figure 5(a) depicts the log–log plot of the decay of total kinetic energy in time for both models, along with the slopes for $n = 1.3$ and 2.5. As it can be seen, both models seem to be able to capture the total energy decay rate quite efficiently. The separation between the inertia- and viscosity-dominated regimes is clearly visible. The slopes on the log–log plots match the theoretical and experimental predictions well. However, in the LM run, the transition to the final phase of the flow is more spread out in time—approximately between $t = 20$ and 60, as opposed to between $t = 30$ and 50 for the DS run.

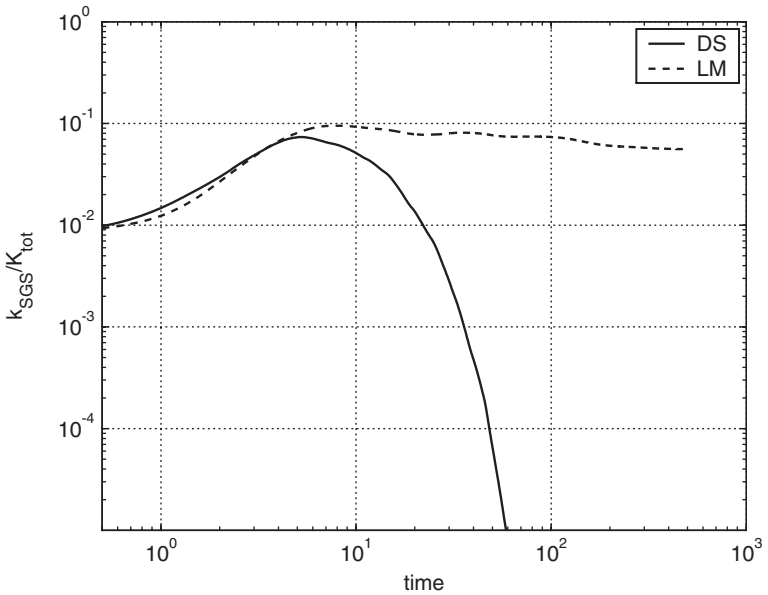

Figure 7. Fraction of total energy stored in subgrid scales for DS and LM sets of models.

Figure 5(b) shows the evolution of the SGS kinetic energy in time for both sets of models. For the LM run, k appears to grow slower but later in time more energy is stored in the subgrid scales. This agrees with Figure 6(a), where we plot the averaged term $-\tau_{ij}\bar{S}_{ij}$ that is responsible for the energy transfer between the resolved and subgrid scales. The non-smoothness of the transfer term profile for the DS run is attributed to a significant amount of backscatter.

Figure 6(b) examines the behaviour of the SGS energy dissipation term in time. Overall, the DS run predicts smaller amount of dissipation than the LM run. This may result in the earlier transition to the viscosity-dominated phase in the LM run.

The most striking difference between the DS and LM models is demonstrated in Figure 7, which shows how the fraction of total kinetic energy stored in the subgrid scales changes in time. It should be noted that the final period of the isotropic decay is characterized by the absence of the inertial range in the energy spectrum [24] thus the fraction of energy stored in the subgrid scales should go to zero as the DIT approaches the final period. This is not captured by the LM set of models, which leaves from 5 to 10% of the energy in subgrid scales at all times, but the DS set of models captures the expected behaviour well.

6. CONCLUSIONS

Three new SGS models that belong to a new class of models—Dynamic Structure Models—are presented and evaluated. The models are tested *a priori* using DNS data for the decaying isotropic turbulence available from the literature and a DNS simulation of a non-reacting incompressible mixing layer. A good agreement between the models and the modelled terms

was found. An *a posteriori* test has been performed as well by simulating decaying isotropic turbulence using LES code with new models. A good match between the energy decay rate, predicted by experimental and theoretical studies, and the results of the LES was found. In *a priori* testing the DS models demonstrate better performance than the models found in the current literature, and the DS models are found to be more robust, i.e., depend less on the base and test LES filter size and shape.

ACKNOWLEDGEMENTS

This work is sponsored in part by the U.S. Army Research Office under contract/grant number DAAD19-00-1-0487 and the Air Force Office of Scientific Research, USAF, under grant number F49620-02-1-0348.

REFERENCES

1. Smagorinsky J. General circulation experiments with the primitive equations. *Monthly Weather Review* 1963; **93**.
2. Rao S, Pomraning E, Rutland CJ. Development of advanced combustion models for diesel engines using large eddy simulation. *Second Joint Meeting of the US Sections of the Combustion Institute*, Oakland, CA, 26–28 March 2001.
3. Pope S. *Turbulent Flows.* Cambridge University Press: Cambridge, 2000.
4. Meneveau C, Katz J. Scale-invariance and turbulent models for large-eddy simulation. *Annual Review of Fluid Mechanics* 2000; **32**:1–32.
5. Ghosal S, Lund TS, Moin P, Aksevoll K. A dynamic localization model for large-eddy simulation of turbulent flows. *Journal of Fluid Mechanics* 1995; **286**:229–255.
6. Kim WW, Menon S. A new dynamics one-equation subgrid-scale model for large-eddy simulation. *AIAA 95-0356*, 2002.
7. Pomraning E, Rutland CJ. Dynamic one-equation nonviscosity large-eddy simulation model. *AIAA Journal* 2002; **40**(4):689–701.
8. Chumakov S, Rutland CJ. Dynamic structure models for scalar flux and dissipation in large eddy simulation. *AIAA Journal* 2004; **42**(6):1132–1139.
9. Goutorbe T, Laurence D, Maupu V. *A priori* tests of a subgrid scale stress tensor model including anisotropy and backscatter effects. In *Direct and Large-Eddy Simulation I, Selected Papers from the 1st ERCOFTAC Workshop on Direct and Large-Eddy Simulation*, Voke *et al.* (eds). Kluwer Academic: Dordrecht, 1994.
10. Bardina J, Ferziger JH, Reynolds WC. Improved subgrid model for large-eddy simulation. *AIAA 80-1357*, 1980.
11. Germano M, Piomelli U, Moin P, Cabot WH. A dynamic subgrid-scale eddy viscosity model. *Physics of Fluids A* 1991; **3**(7):1760–1765.
12. Wray A. Decaying isotropic turbulence. A selection of test cases for the validation of large-eddy simulations of turbulent flows. *AGARD Advisory Report 345*, 63–64.
13. Mason S. Turbulence transport in spatially developing reacting shear layers. *Ph.D. Thesis*, University of Wisconsin-Madison, 2000.
14. Moin P, Squires K, Cabot WH, Lee S. A dynamic subgrid-scale model for compressible turbulence and scalar transport. *Physics of Fluids A* 1991; **3**(11):2746–2757.
15. Pierce C, Moin P. A dynamic model for subgrid-scale variance and dissipation rate of a conserved scalar. *Physics of Fluids* 1998; **12**:3041–3044.
16. Jimenez C, Ducros F, Cuenot B, Bedat B. Subgrid scalar variance and dissipation of a scalar field in large eddy simulations. *Physics of Fluids* 2001; **13**(6):1748–1754.
17. Girimaji SS, Zhou Y. Analysis and modeling of subgrid scalar mixing using numerical data. *Physics of Fluids* 1996; **8**(5):1224–1236.
18. Hinze JO. *Turbulence* (2nd edn). McGraw-Hill: New York, 1975.
19. Comte-Bellot J, Corrsin S. The use of a contraction to improve the isotropy of grid-generated turbulence. *Journal of Fluid Mechanics* 1966; **25**:657–682.
20. Comte-Bellot J, Corrsin S. Simple Eulerian time correlation of full- and narrow-band velocity signals in grid-generated 'isotropic' turbulence. *Journal of Fluid Mechanics* 1971; **48**(2):273–337.

21. Cerutti S, Meneveau C. Statistics of filtered velocity in grid and wake turbulence. *Physics of Fluids* 2000; **12**(5):1143–1165.
22. Mohamed MS, LaRue JC. The decay power law in grid-generated turbulence. *Journal of Fluid Mechanics* **219**:195–214.
23. Menon S, Yeung PK, Kim WW. Effect of subgrid models on the computed interscale energy transfer in isotropic turbulence. *Computers and Fluids* 1996; **25**(2):165–180.
24. Camussi R, Gui G. Experimental analysis of scaling laws in low Re_λ grid-generated turbulence. *Experiments in Fluids* 1996; **20**(3):199–209.

